Published for SISSA by Springer

Received: January 10, 2019
Accepted: March 5, 2019
Published: March 8, 2019

Jet suppression in non-conformal plasma using AdS/CFT

S. Heshmatian[a] **and R. Morad**[b,c]

[a] *Department of Engineering Sciences and Physics, Buein Zahra Technical University, Buein Zahra, Qazvin, Iran*
[b] *UNESCO-UNISA Africa Chair in Nanosciences/Nanotechnology, College of Graduate Studies, University of South Africa (UNISA), Muckleneuk Ridge, P.O.Box 392, Pretoria, South Africa*
[c] *Nanosciences African Network, Materials Research Department, iThemba LABS, P.O.Box 722, National Research Foundation, South Africa*

E-mail: heshmatian@bzte.ac.ir, rmorad@tlabs.ac.za

Abstract: In this paper, suppression of light quark in strongly coupled non-conformal plasmas is studied by using the AdS/CFT correspondence. According to the duality, the well-known falling string profile in the bulk is considered as a light quark moving through the plasma. The maximum distance traversed by an energetic string before falling through the horizon is interpreted as the thermalization distance of light quark in the hot, and strongly coupled plasma. Our numerical results show that the thermalization distance of light quark increases by increasing the deviation from conformal invariance. The relation between this distance and the energy of quark and the temperature of the plasma is analyzed numerically. Moreover, jet quenching parameter is calculated in this non-conformal background and it is found that the jet quenching parameter is decreased by increasing the non-conformality. Our results are compared with the results of $\mathcal{N} = 4$ SYM theory and also some available experimental data.

Keywords: AdS-CFT Correspondence, Gauge-gravity correspondence, Holography and quark-gluon plasmas

ArXiv ePrint: 1812.09374

https://doi.org/10.1007/JHEP03(2019)045

JHEP03(2019)045

Contents

JHEP03(2019)045

1 Introduction

Recent experiments performed at the Relativistic Heavy Ion Collider (RHIC) and the Large Hadron Collider (LHC) have provided spectacular evidences supporting the formation of so-called quark-gluon plasma (QGP), a deconfined state of hadronic matter [1–4]. The experimental discovery, e.g, a very small ratio of shear viscosity to entropy density [5, 6], quenching of high energy partons with large transverse momentum, and elliptic flow etc., indicate that QGP is a strongly coupled plasma whose dynamics after collision is dominated by non-perturbative effects [7, 8]. The perturbative QCD works only in the weak coupling regime, while lattice QCD is the proper tool for understanding the static equilibrium thermodynamics of such strongly coupled plasma. However, none of them allow us to compute some dynamical quantities like transport coefficients, drag force, and jet quenching parameter etc., in the strong coupling regime.

Recently, a novel tool called the "AdS/CFT correspondence" [9–13] provide a powerful tool to study the strongly coupled plasma. The most studied example in the context of AdS/CFT correspondence [7, 14, 15] is the duality between the $\mathcal{N} = 4\,\mathrm{SU}(N_c)$ super-Yang-Mills theory and type IIB string theory on $AdS_5 \times S^5$, which allows one to study this strongly coupled gauge theory in the large N_c limit and large 't Hooft coupling, $\lambda = g^2_{\mathrm{YM}} N_c$. The ratio of shear viscosity over entropy density obtained from this duality is small, $\eta/s = 1/4\pi$ [5, 16, 17] which is consistent with the experimental data [18]. Also, the strong collective behavior observed in very small systems, such as Au-Au collisions at RHIC [19–21], Pb-Pb [22–25], p-Pb [26–28] and p-p [29] collisions at LHC are well described by hydrodynamics from the time and distance scales as a fraction of the (local) inverse temperature [30–35] which is consistent with holographic results [36, 37].

Although the initial temperatures in the most central, high-energy collisions are in the range of quasi-conformal regime, the non-conformal effects become important in the

subsequent evolution and cooling of the produced QGP or in the off-central or lower-energy collisions where the temperature is lower. In fact, Lattice data indicates that the QGP with the temperature range available at high-energy heavy ion collisions (temperatures a few times larger than the critical temperature) is not a fully conformal fluid and bulk viscosity (a purely non-conformal effect) is needed for highly-precise extraction of the shear viscosity of the QGP [38]. Furthermore, hydrodynamics including non-conformal effects successfully described the smaller system such as p-Pb [39] and p-p [40, 41] collisions [42].

There are many attempts to extend the original duality to the theories close to QCD or QGP using either a top-down [43–45] or a bottom-up [46, 47] construction. In the latter, the equations of motion of a five-dimensional supergravity action coupled to a matter content of fields is solved. One may break the conformal invariance even at zero temperature by coupling a scalar field at pure gravity in AdS [48] which is dual to a CFT deformed by a source Λ for a dimension-three operator. This source breaks the scale invariance explicitly and triggers a non-trivial Renormalization Group (RG) flow from an ultraviolet (UV) fixed point to an infrared (IR) fixed point. Usually, the scalar potential coupled to gravity is chosen to mimic the detailed properties of QCD, e.g. [49]. However, the authors in [48] have chosen their potential by simplicity. The UV fixed point is needed to guarantee that we are in the regime where the holographic duality is best understood and the bulk metric is asymptotically AdS. The IR fixed point guarantees that the solutions are regular in the interior and the zero-temperature solution is smooth in the deep IR. Although turning on a source for a relevant operator is the simplest way to break conformal invariance, this simple model exhibits a rich phenomenology. For example, the relaxation of small-amplitude and homogeneous perturbations are studied by computing the spectrum of quasi-normal modes (QNM) and it is shown that the dominant channel for relaxation in this approximation depends on the ratio of T/Λ, where T is the temperature of the system. At small T/Λ the system first EoSizes (the evolution of the energy density and the average pressure towards asymptotic values related to one another by the equation of state (EoS)) and then isotropises. In contrast at large T/Λ, the system first isotropises and subsequently EoSizes [48].

One of the interesting properties of QGP is jet quenching processes in which a high energy parton propagates through the medium, interacts with medium and consequently loses energy. Analysing the energy loss of these energetic partons as they travel throw QGP may reveal extremely valuable information about the dynamics of plasma and may exhibit distinctive properties such as jet-quenching which can be clearly observed at RHIC [1–4] and more recently at LHC [50–52].

In the AdS/CFT correspondence, an external heavy quark with infinite mass can be introduced by adding a fundamental string attached to a flavor brane on the AdS boundary. The string endpoint specifies the heavy quark while the string itself can be considered as a gluonic cloud around the quark. The mass of quark is proportional to the inverse distance of the string endpoint from the boundary, such that light quark or massless quark is mapped into a string attached to a flavor brane which is extended from the boundary to the horizon [53–57].

JHEP03(2019)045

A pair of light quark-anti quark is modelled by an initially point-like open string created close to the boundary with endpoints that are free to fly apart [58, 59]. The initial conditions of the string imply that the string extends in a direction parallel to the boundary as it falls toward the black hole horizon, so it is called the falling string. The maximum stopping distance of the falling string (the maximum distance which a quark with initial energy E can travel) can be used as a phenomenological guideline to estimate the stopping power of the strongly- coupled plasma. This quantity is calculated numerically for many different sets of string initial conditions in a thermal $N = 4$ SYM plasma at a temperature T and it is found that the maximum penetration depth scales as $x_{\max} = \frac{C}{T}\left(\frac{E}{T\sqrt{\lambda}}\right)^{n_{\text{eff}}}$ where C is a constant and $n_{\text{eff}} = 1/3$ [58]. The analogous computation is done in a plasma with non-conformal effect [60] or with anisotropy effect [61] and it is shown that the power of n_{eff} deviates from its conformal isotropic cousin. The constant of proportionality is also important for phenomenological applications as it determines the overall strength of jet quenching. Here, we analyze the maximum stopping distance of light quark by numerical computation of stopping distance for many different sets of string initial conditions in the non-conformal background of [48].

Another interesting experimental observables associated with quark energy lost in the dense hot QGP is the transport coefficient which is called "jet quenching", $\hat{q}$. This observable is defined as the average transverse momentum square transferred from the traversing parton, per unit mean free path [62]. As mentioned before, the quark-antiquark pair in the context of AdS/CFT is mapped to a fundamental string with both endpoints attached to the AdS boundary. The string hangs down to the bulk along the radial direction. The jet quenching parameter $\hat{q}$ is related to the thermal expectation value of the light-like Wilson loop operator [63] corresponding to the trajectory of two endpoints of the string. Several attempts were made to compute this parameter using the AdS/CFT correspondence [63–78]. In this paper, we also study the jet quenching parameter in the introduced non-conformal background. Our results are in good agreement with experimental expectation.

This paper is organised as follows: in section 2 we briefly review the non-conformal background introduced in [48]. In section 3 we discuss the generic falling string solutions and calculate the maximum stopping distance of light quark in the strongly coupled non-conformal plasma. In section 4, we calculate the jet quenching parameter and section 5 is devoted to summary.

2 Non-conformal holographic model

In this section we review the non-conformal holographic model presented by [48]. The action for the five-dimensional Einstein gravity coupled to a scalar field is

$$S = \frac{2}{\kappa_5^2}\int d^5x\sqrt{-g}\left[\frac{1}{4}\mathcal{R} - \frac{1}{2}\left(\nabla\phi\right)^2 - V(\phi)\right], \tag{2.1}$$

where κ_5 is the five-dimensional Newton constant. The considered potential in this model has the following non-trivial rather simple form

$$L^2V = -3 - \frac{3}{2}\phi^2 - \frac{1}{3}\phi^4 + \left(\frac{1}{3\phi_M^2} + \frac{1}{2\phi_M^4}\right)\phi^6 - \frac{1}{12\phi_M^4}\phi^8\,. \tag{2.2}$$

This potential possesses a maximum at $\phi = 0$ (UV fixed point) and a minimum at $\phi = \phi_M$ (IR fixed point) corresponding to two AdS solutions. L is the radius of the AdS solution at the UV whereas the radius of the IR AdS is

$$L_{\rm IR} = \sqrt{-\frac{3}{V(\phi_M)}} = \frac{1}{1+\frac{1}{6}\phi_M^2} L\,. \tag{2.3}$$

The number of degrees of freedom decreases along the flow (from a UV to an IR) because of the fact that $L_{\rm IR} < L$.

The vacuum solutions to the Einstein equations can be easily found

$$ds^2 = e^{2A(r)}\left(-dt^2 + d\mathbf{x}^2\right) + dr^2\,, \tag{2.4}$$

where

$$e^{2A} = \frac{\Lambda^2 L^2}{\phi^2}\left(1-\frac{\phi^2}{\phi_M^2}\right)^{\frac{\phi_M^2}{6}+1} e^{-\frac{\phi^2}{6}}\,, \tag{2.5}$$

$$\phi(r) = \frac{\Lambda L\, e^{-r/L}}{\sqrt{1+\frac{\Lambda^2 L^2}{\phi_M^2} e^{-2r/L}}}\,. \tag{2.6}$$

Here, Λ is an arbitrary constant that breaks conformal invariance. The scalar field is dual to a scalar operator in the dual gauge theory Ø, with different dimension at the UV and IR fixed points. The dimension of this operator at the UV fixed point is $\Delta_{UV} = 3$ while the operator Ø at the IR fixed point has dimension

$$\Delta_{\rm IR} = 6\left(1+\frac{\phi_M^2}{9}\right)\left(1+\frac{\phi_M^2}{6}\right)^{-1}\,. \tag{2.7}$$

So, by increasing ϕ_M the dimension of the scalar operator at the IR fixed point decreases and finally reaches $\Delta_{IR} = 4$ at $\phi_M \to \infty$. One can determine the vacuum expectation values (VEV) of the stress tensor and the scalar operator by studying the behavior of the metric and the scalar field near the boundary. Using the new variable u as $u = L\, e^{-r/L}$, the metric can be rewritten as [79]

$$ds^2 = \frac{L^2}{u^2}\left(du^2 + g_{\mu\nu}\, dx^\mu dx^\nu\right)\,. \tag{2.8}$$

The expectation values of the field theory operators can be readily determined by expanding the metric and the scalar field in powers of u in the $u \to 0$ limit as follows [48]

$$\langle T_{\mu\nu}\rangle = \frac{2L^3}{\kappa_5^2}\left[g_{\mu\nu}^{(4)} + \left(\Lambda^2\,\phi_2 - \frac{\Lambda^4}{18} + \frac{\Lambda^4}{4\phi_M^2}\right)\eta_{\mu\nu}\right]\,, \tag{2.9}$$

$$\langle \text{Ø}\rangle = -\frac{2L^3}{\kappa_5^2}\left(2\Lambda\phi_2 + \frac{\Lambda^3}{\phi_M^2}\right)\,, \tag{2.10}$$

which implies the Ward identity for the trace of the stress tensor

$$\left\langle T_\mu^\mu\right\rangle = -\Lambda\,\langle \text{Ø}\rangle\,. \tag{2.11}$$

JHEP03(2019)045

Since the scalar field is a monotonic function of r, we can use the ϕ as the radial coordinate and consider the following ansatz for black brane solutions of the action in the Eddington-Finkelstein form [49]

$$ds^2 = e^{2A}\left(-h(\phi)d\tilde{t}^{\,2} + d\mathbf{x}^2\right) - 2e^{A+B}L\,d\tilde{t}\,d\phi\,, \tag{2.12}$$

where $h(\phi)$ is the blackening factor which is zero at horizon, $\phi = \phi_H$. The boundary of space is at $\phi = 0$ and ϕ_H is the location of the horizon. With this ansatz, the equations of motion can be written as

$$A''(\phi) - A'(\phi)B'(\phi) + \frac{2}{3} = 0\,, \tag{2.13a}$$

$$4A'(\phi)h'(\phi) - B'(\phi)h'(\phi) + h''(\phi) = 0\,, \tag{2.13b}$$

$$\frac{3}{2}A'(\phi)h'(\phi) + h(\phi)\left(6A'(\phi)^2 - 1\right) + 2e^{2B(\phi)}L^2V(\phi) = 0\,, \tag{2.13c}$$

$$4A'(\phi) - B'(\phi) - \frac{e^{2B(\phi)}L^2V'(\phi)}{h(\phi)} + \frac{h'(\phi)}{h(\phi)} = 0\,, \tag{2.13d}$$

where primes denote $d/d\phi$. It is shown that these four equations can be combined into a master equation of the form [48]

$$\frac{G'(\phi)}{G(\phi) + \frac{4V(\phi)}{3V'(\phi)}} = \frac{d}{d\phi}\log\left(\frac{1}{3G(\phi)} - 2G(\phi) + \frac{G'(\phi)}{2G(\phi)} - \frac{G'(\phi)}{2\left(G(\phi) + \frac{4V(\phi)}{3V'(\phi)}\right)}\right)\,, \tag{2.14}$$

where $G(\phi) = \frac{d}{d\phi}A(\phi)$ is assumed to be a smooth generating function which can be integrated to obtain $A(\phi)$ as

$$A(\phi) = A_0 + \int_{\phi_0}^{\phi} d\tilde{\phi}\, G(\tilde{\phi})\,. \tag{2.15}$$

Integrating the first three equations of eq. (2.13) leads to

$$B(\phi) = B_0 + \int_{\phi_0}^{\phi} d\tilde{\phi}\,\frac{G'(\tilde{\phi}) + 2/3}{G(\tilde{\phi})}\,, \tag{2.16a}$$

$$h(\phi) = h_0 + h_1\int_{\phi_0}^{\phi} d\tilde{\phi}\, e^{-4\,A(\tilde{\phi}) + B(\tilde{\phi})}\,, \tag{2.16b}$$

$$V(\phi) = \frac{h(\phi)\,e^{-2B(\phi)}}{2L^2}\left(1 - 6G(\phi)^2 - \frac{3\,G(\phi)\,h'(\phi)}{2\,h(\phi)}\right)\,. \tag{2.16c}$$

Using the fact that h has a simple zero at the horizon, the eq. (2.13c) and eq. (2.13d) give rise to

$$V(\phi_H) = -\frac{3}{4\,L^2}G(\phi_H)h'(\phi_H)\,e^{-2B(\phi_H)}\,, \tag{2.17a}$$

$$V'(\phi_H) = \frac{1}{L^2}h'(\phi_H)\,e^{-2B(\phi_H)}\,, \tag{2.17b}$$

JHEP03(2019)045

which leads to the solution of $G(\phi)$ at the horizon as

$$G(\phi_H) = -\frac{4}{3}\frac{V(\phi_H)}{V'(\phi_H)}\,. \tag{2.18}$$

So, the near horizon solution of G can be read as

$$G(\phi) = -\frac{4}{3}\frac{V(\phi_H)}{V'(\phi_H)} - \frac{2}{3}\left(1 - \frac{V(\phi_H)V''(\phi_H)}{V'(\phi_H)^2}\right)(\phi - \phi_H) + O\left[(\phi - \phi_H)^2\right]\,. \tag{2.19}$$

On the other hand, near boundary ($\phi \to 0$) solution of G turns out to be

$$G(\phi) = \frac{1}{\Delta - 4}\frac{1}{\phi} + \cdots\,, \tag{2.20}$$

where Δ is the dual operator scaling dimension which is 3 for the choice of potential eq. (2.2) as mentioned above. Substituting the eq. (2.20) into the eq. (2.15) and requiring that A must be finite at the boundary, the function A is obtained

$$A(\phi) \simeq \frac{1}{\Delta - 4}\,\log(\phi)\,. \tag{2.21}$$

Comparing this equation with eq. (2.15) at the limit of $\phi_0 \to \phi_H$ lead to

$$A_H \equiv A(\phi_H) = \log\left(\frac{\phi_H}{\Delta - 4}\right) + \int_0^{\phi_H} d\phi\left(G(\phi) - \frac{1}{(\Delta - 4)\phi}\right)\,, \tag{2.22}$$

and finally A can be expressed as

$$A(\phi) = A_H + \int_{\phi_H}^{\phi} d\tilde{\phi}\, G(\tilde{\phi})\,. \tag{2.23}$$

There is a residual gauge freedom in the ansatz of metric $dr = \pm e^B\, d\phi$. As ϕ increases from zero to ϕ_H, the radial coordinate r decreases from ∞ to a finite value. Therefore the minus sign is meaningful. The leading asymptotic behavior of metric functions at large r is

$$A \approx \frac{r}{L} \qquad h \approx 1 \qquad \phi \approx (\Lambda L)^{4-\Delta} e^{(\Delta-4)A}\,. \tag{2.24}$$

Accordingly, the asymptotic behavior of generating function at large r becomes

$$G = \frac{dA}{d\phi} = \frac{dr}{d\phi}\frac{dA}{dr} \approx -e^B\frac{1}{L}\,. \tag{2.25}$$

By considering the lower limit of the integral in the eq. (2.16a) to be ϕ_H and manipulating the equation, one can find the following relation

$$B(\phi) - B(\phi_H) = \log\frac{G(\phi)}{G(\phi_H)} + \frac{2}{3}\int_{\phi_H}^{\phi}\frac{d\tilde{\phi}}{G(\tilde{\phi})}\,. \tag{2.26}$$

Substituting $B(\phi)$ from eq. (2.25) into the above equation, $B(\phi_H)$ is obtained as follows

$$B_H \equiv B(\phi_H) = \log(-G(\phi_H)) + \frac{2}{3}\int_0^{\phi_H}\frac{d\phi}{G(\phi)}\,, \tag{2.27}$$

JHEP03(2019)045

and finally we get

$$B(\phi) = B_H + \int_{\phi_H}^{\phi} d\tilde{\phi} \frac{G'(\tilde{\phi}) + 2/3}{G(\tilde{\phi})} \,. \tag{2.28}$$

In the last step, one can obtain the function $h(\phi)$ from eq. (2.13c) and eq. (2.13d) as follows

$$h(\phi) = -\frac{e^{2B(\phi)} L^2 \left(4V(\phi) + 3G(\phi)V'(\phi)\right)}{3G'(\phi)} \,. \tag{2.29}$$

The thermodynamical quantities of the background are expressed as

$$L\,T = \frac{A(\phi_H) - B(\phi_H)}{4\pi} \,, \qquad s = \frac{2\pi}{\kappa_5^2} e^{3A(\phi_H)} \,. \tag{2.30}$$

Substituting the metric functions at the horizon leads to the following form for the temperature and entropy of the plasma

$$T = -\Lambda \frac{L^2 V(\phi_H)}{3\pi\phi_H} \exp\left\{ \int_0^{\phi_H} d\phi \left(G(\phi) + \frac{1}{\phi} + \frac{2}{3G(\phi)} \right) \right\} \,, \tag{2.31}$$

$$s = \frac{2\pi}{\kappa_5^2} \frac{\Lambda^3}{{\phi_H}^3} \exp\left\{ 3 \int_0^{\phi_H} d\phi \left(G(\phi) + \frac{1}{\phi} \right) \right\} \,. \tag{2.32}$$

The non-conformal behavior of the thermodynamics of the dual theory can be identified by studying the entropy, the speed of sound, the ratio of bulk over shear viscosity and the violation of Buchel's bound. In figure 1a, we plot the ratio of non-conformal to the conformal entropy in terms of temperature. At high and low temperature, the entropy of the theory is the same as the conformal theory and scale as T^3.

The square of the speed of sound can be obtained from the inverse of the logarithmic derivative of the entropy as

$$\frac{1}{c_s^2} = \frac{d\log s}{d\log T} \,. \tag{2.33}$$

The deviation of the speed of sound from its conformal value ($c_s = 1/\sqrt{3}$) is depicted in the figure 1b as a function of temperature. At low and high temperatures, this quantity reaches its conformal value while the deviation gets larger by increasing ϕ_M at intermediate temperatures. The ratio of shear viscosity η to entropy has a universal value of $\eta/s = 1/4\pi$ for all theories with a two-derivative gravity dual [6]. The bulk viscosity, ζ can be determined from the dependency of the entropy to the value of the scalar field at the horizon [80]

$$\frac{\zeta}{\eta} = 4 \left(\frac{d\log s}{d\phi_H} \right)^{-2} \,, \tag{2.34}$$

which is zero in any conformal field theory. This ratio has been shown in the figure 1c as a function of temperature for different values of ϕ_M. The behavior of this quantity as a function of temperature is similar to that of the speed of sound. At low temperatures, the violation of this ratio from Buchel's bound is shown in the figure 1d.

JHEP03(2019)045

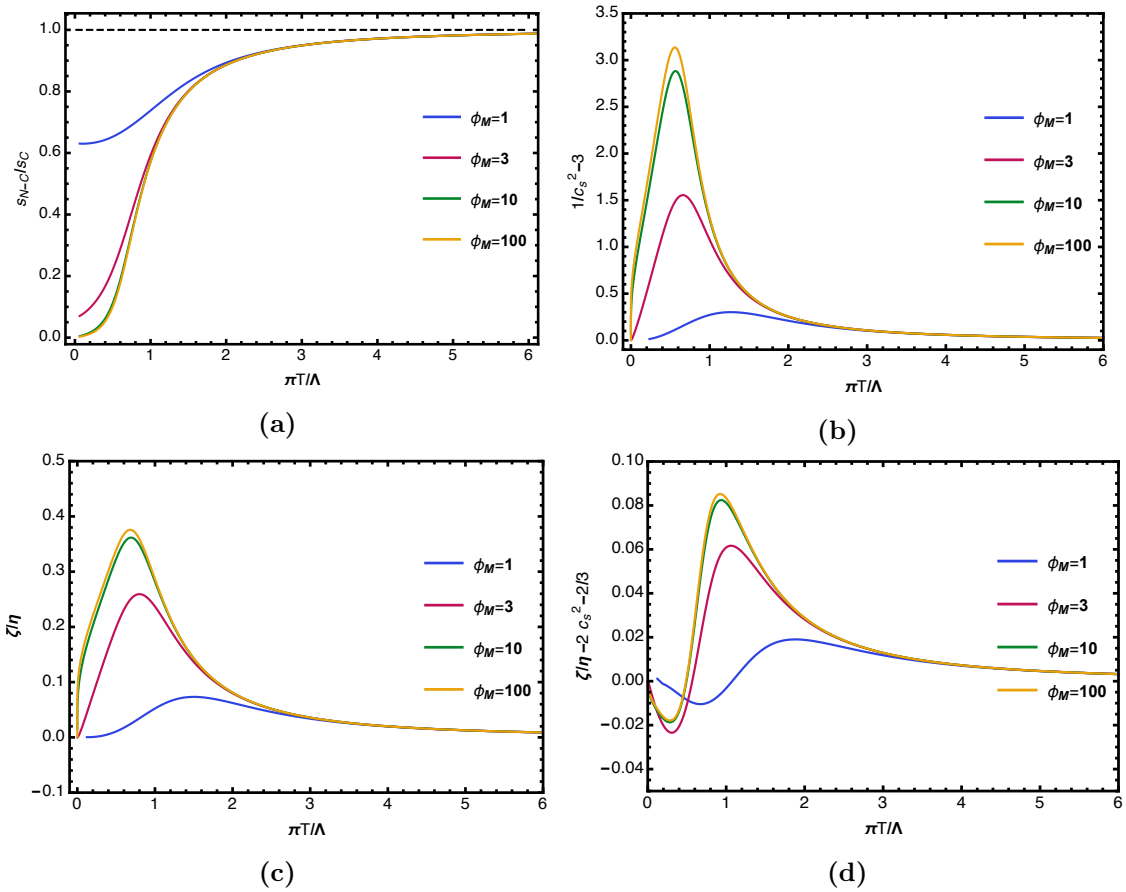

Figure 1. (Color online) (a) The ratio of non-conformal to the conformal entropy, (b) inverse speed of sound square, (c) ratio of bulk to shear viscosity, (d) violation of Buchel's bound as a function of temperature for different values of ϕ_M.

3 Light quark maximum stopping distance

We are interested to study the propagation of energetic excitations which resemble quark jets through the strongly coupled non-conformal plasma. These excitations are considered as open string configurations with high energy, moving through the bulk of AdS space. The maximum stopping distance of these strings, the quantity which is not sensitive to the precise initial conditions, can be used as a phenomenological guideline to estimate the stopping power of the strongly- coupled plasma.

In this section, we first briefly review the string configuration dual to a light quark jet in the non-conformal background and then numerically calculate the maximum stopping distance traversed by a quark with initial energy E.

3.1 String configuration

We rewrite the black brane solution of eq. (2.12) in Poincare coordinates to study the non-conformality effect on the dynamics of light quark jet moving in a strongly coupled plasma. According to the gauge/gravity duality, quarks moving through a medium are dual to open

JHEP03(2019)045

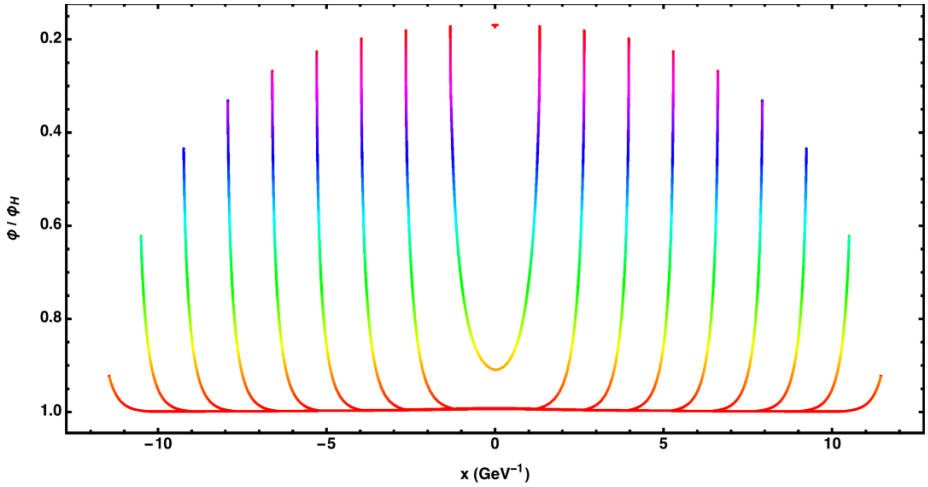

Figure 2. The typical falling string profiles moving in the $x - \phi$ plane in the non-conformal background eq. (2.12) with $\phi_M = 3$ and $T = 0.265\,\text{GeV}$. The string is created at the point $\phi_c = 0.2$ and evolved to the extended object by time evolution. The quark, corresponding to the half of the string, has the energy of 100 GeV and the small positive virtuality as defined in eq. (3.13).

strings moving in the 10-d gravitational background. Flavor D-branes are added to the background in the probe limit (do not back-react on the background metric) to describe the fundamental matter of the field theory. These branes fill the $4D$ Minkowski space and extend along the radial coordinate from the boundary at $\phi = 0$ down to the location of the horizon at $\phi = \phi_H$ and wraps an S^3 of the S^5 sphere. In the AdS/CFT dictionary, quark-antiquark pairs in the field theory side are dual to open strings whose endpoints are attached to the D-brane.

In this paper, we consider a back-to-back jet pair created in the medium which can be regarded as a string created at a point, extends in space-time and falls toward the horizon. The profile evolution of a typical string for various times has been shown in figure 2. In this setup, the two endpoints of the string move away from each other and the total spatial momentum of the string vanishes. The string embedding function is $X^\mu(\tau,\sigma) \mapsto (t(\tau,\sigma), x(\tau,\sigma), 0, 0, \phi(\tau,\sigma))$ and for an open string created in a point $\phi = \phi_c$ at a time t_c, the profile is given by

$$t(0,\sigma) = t_c\,, \quad x(0,\sigma) = 0\,, \quad \phi(0,\sigma) = \phi_c, \tag{3.1}$$

where t_c is the time for which the string becomes an extended object from a point and $\sigma \in [0,\pi]$.

The Nambu-Goto action becomes singular for falling string at late times, therefore we use the Polyakov action in which additional degrees of freedom are involved by a nontrivial worldsheet metric η^{ab} and the equations of motion are well-behaved everywhere on the worldsheet [53, 58, 81]. The Polyakov action for the string has the following form

$$S_P = -\frac{T_0}{2}\int d^2\sigma\,\sqrt{-\eta}\,\eta^{ab}\,\partial_a X^\mu \partial_b X^\nu\, G_{\mu\nu}\,. \tag{3.2}$$

JHEP03(2019)045

Canonical momentum densities associated with the string can be obtained by varying the action with respect to the derivatives of the embedding functions,

$$\Pi^a_\mu(\tau,\sigma) \equiv \frac{1}{\sqrt{-\eta}}\,\frac{\delta S_{\rm P}}{\delta(\partial_a X^\mu(\tau,\sigma))} = -T_0\,\eta^{ab}\,\partial_b X^\nu\,G_{\mu\nu}, \tag{3.3}$$

and the equations of motion are obtained by variation of the Polyakov action with respect to the embedding functions X^μ as

$$\begin{aligned}\partial_a\big[\sqrt{-\eta}\,\eta^{ab}\,G_{\mu\nu}\,\partial_b X^\nu\big] &= \frac{1}{2}\sqrt{-\eta}\,\eta^{ab}\frac{\partial G_{\nu\rho}}{\partial X^\mu}\,\partial_a X^\nu \partial_b X^\rho \\ \Longleftrightarrow \qquad \nabla_a\,\Pi^a_\mu &= -\frac{T_0}{2}\,\eta^{ab}\frac{\partial G_{\nu\rho}}{\partial X^\mu}\,\partial_a X^\nu \partial_b X^\rho.\end{aligned} \tag{3.4}$$

We choose the following worldsheet metric

$$\|\eta_{ab}\| = \begin{pmatrix} -\Sigma(\phi) & 0 \\ 0 & \Sigma(\phi)^{-1} \end{pmatrix}, \tag{3.5}$$

where Σ is called the stretching function and generally can be an arbitrary function of worldsheet embedding functions. We found that choosing the stretching function of the form

$$\Sigma(\phi) = \left(\frac{e^{A(\phi)}}{e^{A(\phi_c)}}\right)^a \left(\frac{h(\phi)}{h(\phi_c)}\right)^b \tag{3.6}$$

would cancel the singularities and equations of motion remain well behaved everywhere on the worldsheet. We choose values of a and b in the range of 1 to 5 depends on the string initial conditions. The constraint equation is obtained by varying the Polyakov action, eq. (3.2) with respect to η^{ab} which reduces to $\dot{X}^2(0,\sigma) = 0$ at initial time by considering a string with point-like initial condition. Combining the open string boundary condition and constraint equation, the initial profile must satisfy the following conditions

$$\dot{x}'(0,\sigma^*) = \dot{\phi}'(0,\sigma^*) = 0. \tag{3.7}$$

The below initial conditions (IC) obey all necessary conditions and assures the physical requirements for the non-conformal background

$$\begin{aligned}\dot{x}(0,\sigma) &= A\,\phi_{\rm c}\cos\sigma\,, \\ \dot{\phi}(0,\sigma) &= \phi_{\rm c}\,\left(1-\cos 2\sigma\right), \\ \dot{t}(0,\sigma) &= \sqrt{\frac{g_{xx}(\phi_c)\,\dot{x}^2 + g_{\phi\phi}(\phi_c)\,\dot{\phi}^2}{-g_{tt}(\phi_c)}}\,,\end{aligned} \tag{3.8}$$

where ϕ_c and A are free parameters related to the energy and momentum of the dual quark in the field theory side. The IC are chosen such that the string is long-lived and yields to the stable numerical solutions. Moreover, most of the string's energy and momentum are concentrated near its endpoints. These IC yield a symmetric string profile about $x = 0$ at all times, since $\dot{x}(0,\sigma)$ is antisymmetric about $\sigma = \pi/2$ while $\dot{\phi}(0,\sigma)$ is symmetric. An

JHEP03(2019)045

explicit check of any numerical solution was performed to be assured that all numerical solutions respect the equation of constraint for all τ.

The non-conformal background geometry $G^{\mu\nu}$ depends only on ϕ, hence for μ corresponding to $(t, \vec{x})$ one can write

$$\nabla_a \Pi^a_\mu = 0\,, \tag{3.9}$$

which means that the momentum densities Π^a_μ are conserved Noether currents on the related worldsheet. Therefore, the total energy of the falling string is constant and equals to its initial energy

$$\begin{aligned} E_{\text{string}} &= -\int_0^\pi d\sigma\, \sqrt{-\eta}\, \Pi^\tau_t(0,\sigma) \\ &= \frac{\lambda}{2\pi}\int_0^\pi d\sigma\, \sqrt{g_{tt}(\phi_c)\left(g_{xx}(\phi_c)\,\dot{x}(0,\sigma)^2 + g_{\phi\phi}(\phi_c)\,\dot{\phi}(0,\sigma)^2\right)}\,, \end{aligned} \tag{3.10}$$

and the total energy of light quark is obtained from

$$E_q = \frac{1}{2} E_{\text{string}}\,. \tag{3.11}$$

The total momentum of the string is conserved in x-direction and can be found from the string IC as

$$P_q = \frac{\lambda}{2\pi}\int_0^{\pi/2} d\sigma\; g_{xx}(\phi_c)\,\dot{x}(0,\sigma)\,. \tag{3.12}$$

Here, the total momentum of the string in x-direction is completely symmetric about $\sigma = \pi/2$ and equals to zero. Therefore, the quark momentum equals to the anti-quark momentum with a minus sign. The string energy and momentum are determined by two parameters A and ϕ_c in the string initial condition. These parameters are translated into the virtuality of the jet created in the non-conformal QGP obtained from

$$Q^2 \equiv E_q^2 - P_q^2\,. \tag{3.13}$$

The solution of eq. (3.4) for a typical string with $E = 100\,\text{GeV}$ in the non-conformal background eq. (2.12) with $\phi_M = 3$ is plotted in figure 2. The temperature of the plasma is about $T = 0.265\,\text{GeV}$. The dynamics of two halves of the string are exactly alike, one moving in the opposite direction of the another one. As we expected, the two endpoints of the string move away from each other as the string extends along the (x, ϕ) direction and falls toward the horizon.

3.2 Maximum stopping distance

Numerical studies, figure 3 show that the traversed distance of a quark with a specific energy in the plasma before thermalizing depends strongly on the chosen initial condition of the dual string, i.e. the initial distance from the boundary. Since there is no known map between the string IC and the actual field theory quantities, we aim to study a quantity which is insensitive to these IC at the string side. The stopping distance which is called

JHEP03(2019)045

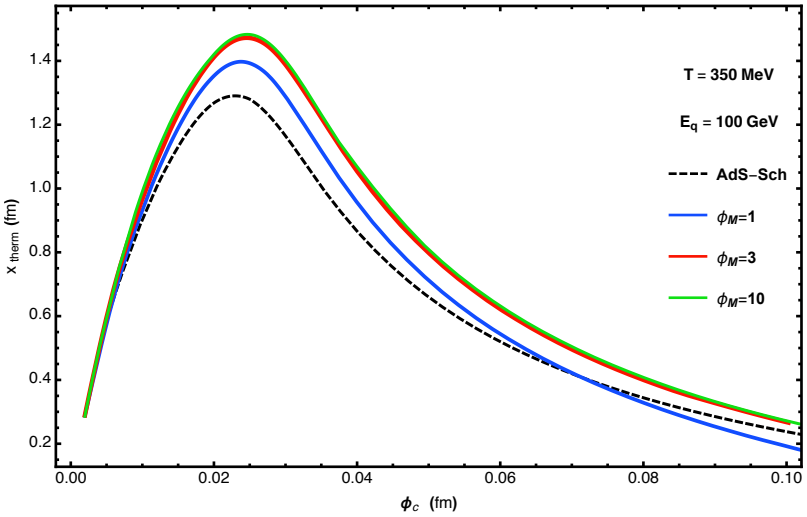

Figure 3. (Color online) The maximum stopping distance of the jet moving in the plasmas versus to its initial distance from the boundary located at $\phi = 0$. The non-conformal plasma has the same temperature as the conformal plasma, $T = 350\,\text{MeV}$. In all cases, the quark has 100 GeV energy but created at a different radial distance from the boundary. The dashed black line is the stopping distance in the AdS-Sch background, while the blue, red and green lines are stopping distance in the non-conformal plasmas with $\phi_M = 1$, 3 and 10, respectively. The stopping distance increases by increasing ϕ_M in the medium ranges of ϕ_c where it is maximum.

the thermalization distance, x_{therm} is defined as the length along the x-direction between two points at which the point-like string originates and falls into the black hole horizon respectively. On the field theory side of the duality, x_{therm} corresponds to the length of the plasma traversed before the jet becomes completely thermalized (i.e. indistinguishable from the plasma). We are looking for the maximum distance a quark with the energy E can travel before thermalizing independent of the exact IC of the string. Although this quantity is not enough to calculate observables such as R_{AA} or v_2 in general, it can be used as a phenomenological guideline to estimate the stopping power of the strongly-coupled plasma.

In order to compare the results of the jet stopping distance in non-conformal plasma with the results of conformal AdS-Sch, we can either fix the temperature or the entropy of the non-conformal plasma with the AdS-Sch ones. In figure 4 we plot the rescaled entropy of the non-conformal theory with different ϕ_M compared to the conformal entropy in terms of temperature. The intersection of black dashed lines shows the entropy of the AdS-Sch metric with $T = 265\,\text{MeV}$ as a reference point. This figure indicates that if we fix the temperature and increase ϕ_M (moving along the vertical dashed black line), the entropy of the non-conformal theory decreases. On the other hand, increasing ϕ_M on the line of fixed entropy (moving along the horizontal dashed black line) give rise to the non-conformal theories with higher temperature.

In figure 5, and figure 6 we numerically compute the stopping distance for many different sets of string initial conditions in the backgrounds with different non-conformal parameters. In these figures, each point shows the logarithm of stopping distance of a string with a specific initial condition in terms of logarithm of its initial energy. Black dots show

JHEP03(2019)045

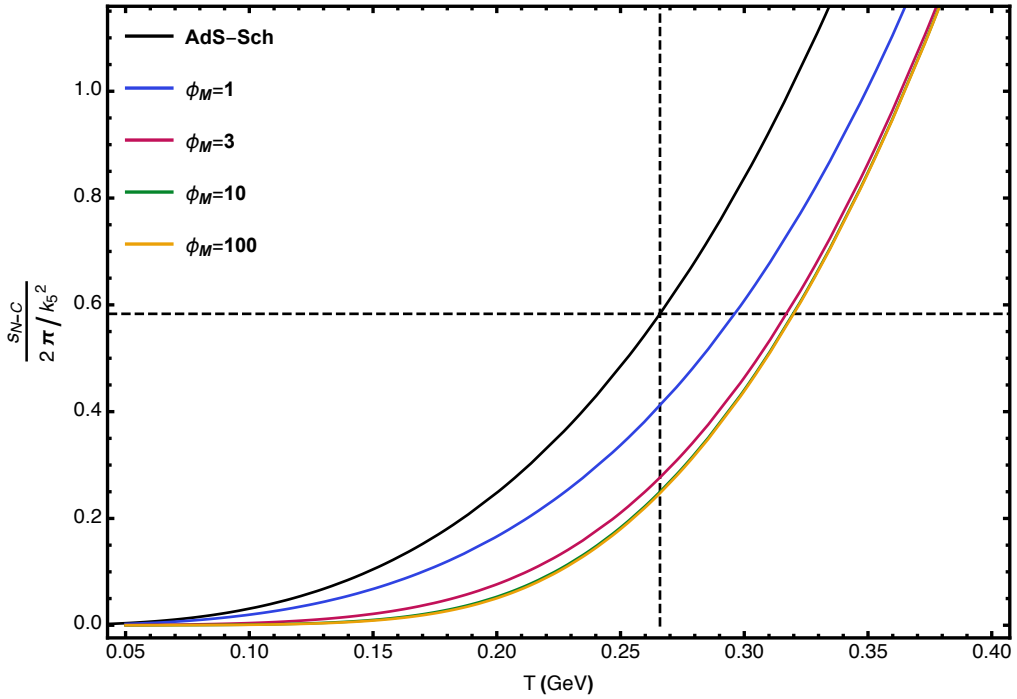

Figure 4. (Color online) The rescaled entropy of the non-conformal theory with different ϕ_M compared with the conformal entropy in terms of temperature. The intersection of two dashed black lines shows an AdS-Sch background with $T = 265\,\mathrm{MeV}$. We study the non-conformality effect on our results by moving away from this point along the either vertical (same temperature) or horizontal (same entropy) dashed black lines.

the strings in the AdS-Sch metric, while the blue triangles, red stars, and green diamonds correspond to strings in the non-conformal backgrounds with $\phi_M = 1$, $\phi_M = 3$, and $\phi_M = 10$, respectively. In the figure 5, all plasmas have the same temperature, while in the figure 6 the entropy of the backgrounds is fixed. The interesting point is that the stopping distance increases by increasing the deviation from conformality when the temperature of the background is fixed. However, it decreases if the entropy of the background is fixed. As explained in figure 4, by fixing the entropy and increasing the ϕ_M, the plasma becomes hotter which leads to a larger jet suppression.

As clearly shown in these figures, the dynamics of the string is a multi-variable quantity depends on the both string IC and background thermodynamics, but all data points for each set of data fall below the solid lines. These lines display the maximum stopping distance of the light quark in the corresponding medium, i.e. the maximum distance that a quark with the energy of E can travel in the medium before thermalization. It is shown that this distance in the conformal background scales like $E^{1/3}$ for large enough energies [58]. In fact, numerical results show that the maximum stopping distance for a given energy depends on the energy of the quark and the temperature of plasma as follows

$$x_{\max} = \frac{\mathcal{C}}{T}\left(\frac{E}{T\sqrt{\lambda}}\right)^{n_{\text{eff}}}, \tag{3.14}$$

JHEP03(2019)045

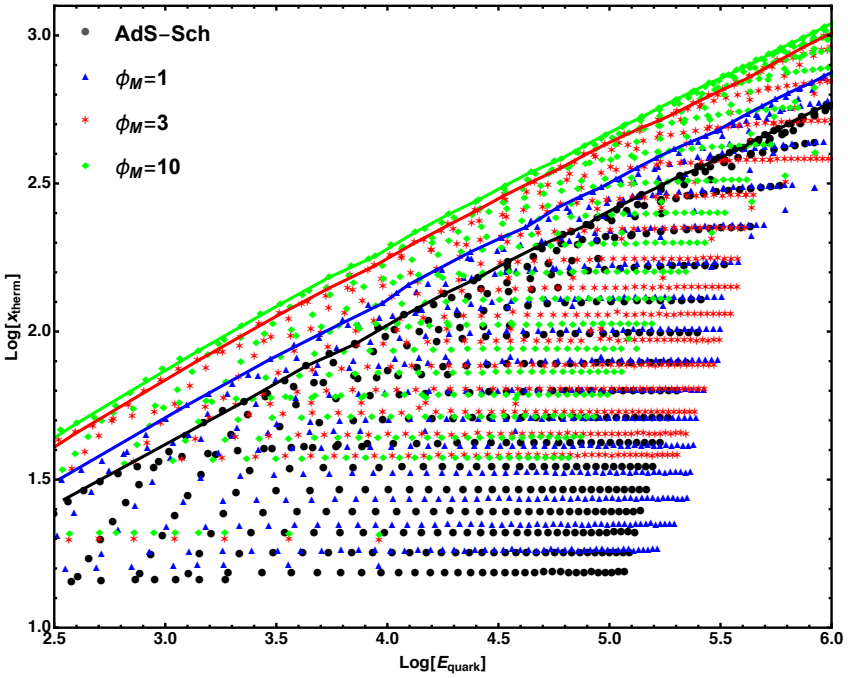

Figure 5. (Color online) The stopping distance of the jet (GeV^{-1}) in terms of its energy (GeV) moving in the non-conformal backgrounds with different ϕ_M. All of the non-conformal backgrounds have the same temperature as the AdS-Sch temperature sets to be 265 MeV. For each set of data, all data points fall below the solid line which determines the maximum stopping distance of the quark in terms of its energy.

which $\mathcal{C}$ and $n_{\rm eff}$ are estimated to be 0.526 and 1/3 in the AdS-Sch case, respectively [58]. We explore this relation with our numerical results and estimate the values of $\mathcal{C}$ and $n_{\rm eff}$ in the case of non-conformal plasma. We fit our data in the AdS-Sch with eq. (3.14) by fixing $\mathcal{C} = 0.526$. The estimated $n_{\rm eff}$ is less than 1/3 for the available energies at RHIC or LHC but it approaches to this value at very high energies.

In figure 7, the $n_{\rm eff}$ is calculated by fitting the numerical results to the eq. (3.14) by considering $\mathcal{C} = 0.45$ for all non-conformal metrics and $\mathcal{C} = 0.526$ for the AdS-Sch metric. In fact, these constants give rise to a more precise fit to the numerical results. Again, in figure 7a all backgrounds have the same temperature and in figure 7b they have the same entropy. In general, increasing the deviation from conformal invariance increases the stopping distance of jet of light quark.

4 Jet quenching

To calculate the jet quenching parameter for the non-conformal theory, we use the thermal expectation value of a close light-like Wilson loop [82]

$$\langle W^A(\mathcal{C})\rangle \approx \exp\left[-\frac{1}{4\sqrt{2}}\hat{q}\, L^-\, L^2\right], \tag{4.1}$$

JHEP03(2019)045

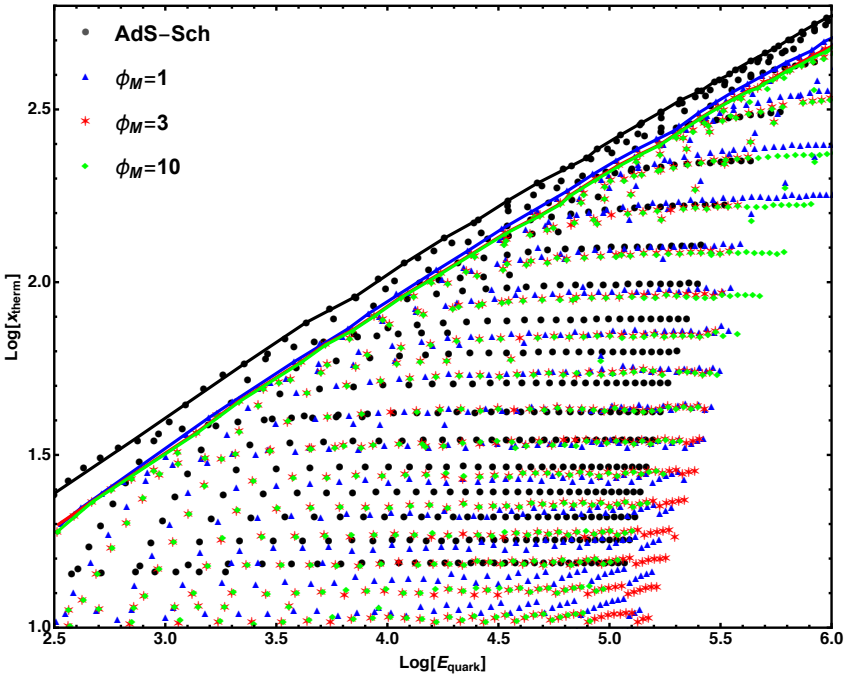

Figure 6. (Color online) The stopping distance of the jet (GeV^{-1}) in terms of its energy (GeV) moving in the non-conformal backgrounds with different ϕ_M. All of the non-conformal backgrounds have the same entropy as the AdS-Sch entropy. For each set of data, all data points fall below the solid line which determines the maximum stopping distance of the quark in terms of its energy.

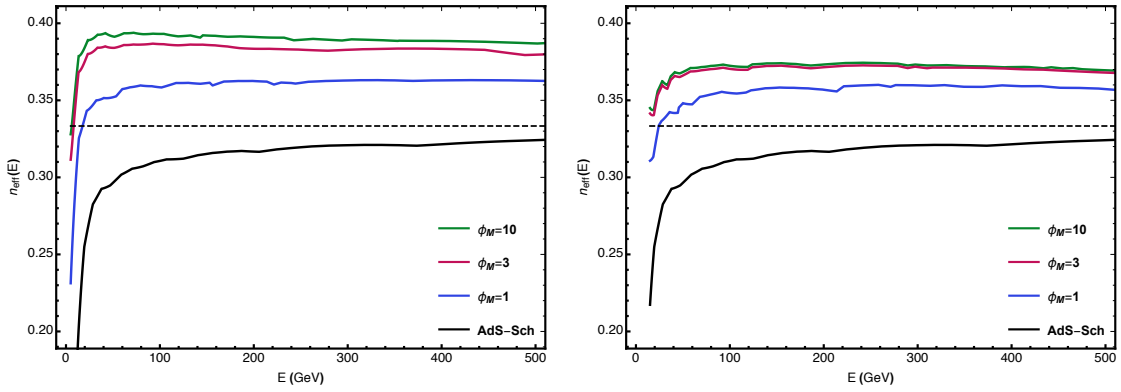

(a) **(b)**

Figure 7. (Color online) (a) The effective power in eq. (3.14) in non-conformal plasmas with the same temperature as the AdS-Sch temperature. (b) The effective power in eq. (3.14) in non-conformal plasmas with the same entropy as the AdS-Sch entropy.

where L is the transverse distance (conjugate to the transverse momentum of the radiated gluons) and L^- is the light-cone distance (conjugate to partons with relativistic velocities). This equation is valid for $L^- \gg L$. In the gravity side, the thermal expectation value of the Wilson loop $\langle W^F(\mathcal{C})\rangle$ can be obtained by using the action of the extremal surface as [83–87]

$$\langle W^F(\mathcal{C})\rangle = \exp\left[-S_I(\mathcal{C})\right] , \tag{4.2}$$

JHEP03(2019)045

where S_I is the normalized action after subtracting the self energy of the $q\bar{q}$ pair from the Nambu-Goto action of the string worldsheet. As in the large N_c limit, $\mathrm{Tr}_{(Adj.)} = \mathrm{Tr}^2{}_{(Fund.)}$, one can write

$$\hat{q} = \frac{8\sqrt{2}S_I}{L^- L^2}. \tag{4.3}$$

In the light-cone coordinates, $x^\pm = (t \pm x_1)/\sqrt{2}$, the non-conformal background of eq. (2.12) becomes

$$\begin{aligned} ds^2 &= -e^{2A}(1+h(\phi))dx^+dx^- + e^{2A}\left(dx_2{}^2 + dx_3{}^2\right) \\ &\quad + \frac{e^{2A}}{2}\left(1-h(\phi)\right)\left(dx^{+2} + dx^{-2}\right) + \frac{e^{2B}}{h}d\phi^2 \\ &\equiv G_{\mu\nu}dx^\mu dx^\nu\,. \end{aligned} \tag{4.4}$$

The string parametrization is $x^\mu(\tau,\sigma)$ where $\sigma^\alpha = (\tau,\sigma)$ is the worldsheet coordinates. The Nambu-Goto action of the string is

$$S_{\mathrm{NG}} = \frac{1}{2\pi\alpha'}\int d\sigma d\tau\,\sqrt{\det g_{\alpha\beta}}, \tag{4.5}$$

where $g_{\alpha\beta}$ is the induced metric on the string worldsheet and (τ,σ) are set to be (x^-, x_2). L is considered to be the contour length along x_2-direction and L^- to be its length along τ-direction. The boundary conditions are $\phi\left(\pm\frac{L}{2}\right) = 0$ and $x_3(\sigma)$ and $x^+(\sigma)$ coordinates are constant. Then the action of eq. (4.5) reads

$$S_{\mathrm{NG}} = \frac{2L^-}{2\pi\alpha'}\int_0^{\frac{L}{2}} d\sigma\,\sqrt{\frac{e^{4A}(1-h(\phi))}{2}}\sqrt{1+\frac{e^{2(B-A)}}{h(\phi)}\,\phi'^2}\,, \tag{4.6}$$

where prime denotes the derivative with respect to σ. Since the Lagrangian density is time independent, the Hamiltonian of the system is constant

$$\mathcal{L} - \phi'\frac{\partial\mathcal{L}}{\partial\phi'} = \Pi_\phi \tag{4.7}$$

and one can obtain the following equation for ϕ'

$$\phi' = \frac{\partial\phi}{\partial\sigma} = \frac{e^{A-B}}{\sqrt{2}\Pi_\phi}\sqrt{h(\phi)\left(e^{4A}(1-h(\phi)) - 2\Pi_\phi{}^2\right)}. \tag{4.8}$$

Integrating equation eq. (4.8) leads to

$$\frac{L}{2} = \sqrt{2}a_0\Pi_\phi + \mathcal{O}(\Pi_\phi{}^3), \tag{4.9}$$

where

$$a_0 = \int_{\phi_H}^0 d\phi\frac{e^{B-3A}}{\sqrt{h(\phi)(1-h(\phi))}}\,. \tag{4.10}$$

Here, we have used the fact that for small length L, the constant Π_ϕ is small and its higher order terms are negligible. Substituting eq. (4.8) into eq. (4.6) and expanding for small Π_ϕ yields to

$$S_{\mathrm{NG}} = \frac{L^-}{\sqrt{2}\pi\alpha'}\int_{\phi_H}^0 d\phi\sqrt{\frac{1-h(\phi)}{h(\phi)}}e^{A+B}\left(1+\frac{e^{-4A}\,\Pi_\phi{}^2}{1-h(\phi)}+\ldots\right). \tag{4.11}$$

JHEP03(2019)045

This action diverges and we should subtract the self energy of two disconnected strings whose worldsheets are located at $x_2 = \pm\frac{L}{2}$ and extended from $\phi = 0$ to $\phi = \phi_H$

$$S_0 = \frac{2L^-}{2\pi\alpha'}\int_{\phi_H}^{0} d\phi\sqrt{g_{--}g_{\phi\phi}} = \frac{L^-}{\sqrt{2}\pi\alpha'}\int_{\phi_H}^{0} d\phi\, e^{A+B}\sqrt{\frac{1-h(\phi)}{h(\phi)}}\,. \tag{4.12}$$

The normalized action is then written as

$$S_I = S_{\rm NG} - S_0 \equiv \frac{L^- L^2}{8\sqrt{2}\pi\alpha' a_0}\,. \tag{4.13}$$

Inserting eq. (4.13) into eq. (4.3) leads to the following expression for the jet quenching parameter of the non-conformal theory

$$\hat{q}_{\rm NC} = \frac{\sqrt{\lambda}}{\pi R^2 a_0}, \tag{4.14}$$

where a_0 is the numerical integral of eq. (4.10). Here, we have used the relation between the string tension and the 't Hooft coupling $\frac{R^2}{\alpha'} = \sqrt{\lambda}$.

For $\mathcal{N} = 4$ supersymmetric Yang-Mills theory in the large N_c and large λ limits, the jet quenching parameter is [88]

$$\hat{q}_{\rm SYM} = \frac{\pi^{3/2}\Gamma\left(\frac{3}{4}\right)}{\Gamma\left(\frac{5}{4}\right)}\sqrt{\lambda}\, T^3, \tag{4.15}$$

To understand how non-conformality affects the jet quenching parameter, we calculate eq. (4.14) for different values of ϕ_M numerically. Here, we have taken the 't Hooft coupling $\lambda = 5.5$ for numerical estimates. The ratio of jet quenching in non-conformal background to its conformal value in terms of temperature is shown in figure 8a for $\phi_M = 1$ (blue curve), $\phi_M = 3$ (red curve) and $\phi_M = 10$ (green curve). The plot shows that for each value of ϕ_M, the ratio of $\hat{q}_{\rm NC}/\hat{q}_{\rm SYM}$ starts from a finite value and approaches to 1 at higher temperature where conformality is dominant. This behavior reflects the fact that deviations from conformality are magnificent at lower temperatures and suppress at higher temperatures. Also, increasing the values of ϕ_M, decreases the values of jet quenching (and hence the ratio is decreased). In figure 8b, the temperature dependency of the jet quenching parameter is shown for $\phi_M = 1$ (blue curve), $\phi_M = 3$ (red curve), $\phi_M = 10$ (green curve) as well as $\mathcal{N} = 4$ SYM theory (dashed curve). Two black circles with error bars are the corresponding absolute values of $\hat{q}$ for a 10 GeV quark jet in the most central Au-Au collisions at RHIC with the highest temperature $T = 0.37$ GeV and Pb-Pb collisions at LHC with the highest temperature $T = 0.47$ GeV [89]. Both temperatures are rescaled due to the fact that the number of degrees of freedom in the non-conformal theory is more than those of 3 favor QCD and one can use $T_{\rm NC} \approx T_{\rm SYM} = 3^{-1/3}T_{\rm QCD}$ [89].

In table 1, the numerical values of the jet quenching parameter is shown for $\mathcal{N} = 4$ SYM theory, non-conformal background ($\phi_M = 1$, $\phi_M = 3$ and $\phi_M = 10$) and experimental data from RHIC and LHC. $\hat{q}$ values are in the units of GeV^2/fm. It can be seen that the jet quenching results from non-conformal background are in a good agreement with the

JHEP03(2019)045

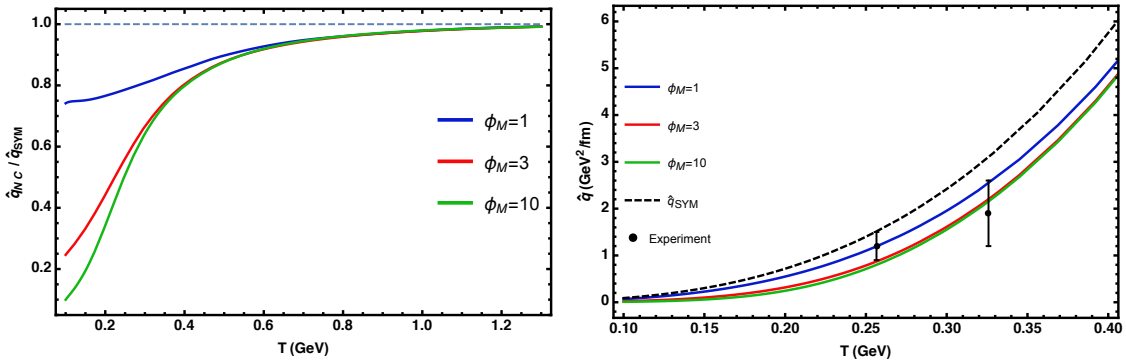

(a) **(b)**

Figure 8. (a) The ratio of $\hat{q}_{\rm NC}/\hat{q}_{\rm SYM}$ in terms of temperature for different ϕ_M. (b) Jet quenching parameter for $\mathcal{N}=4$ SYM theory and non-conformal theory with different ϕ_M. The circles indicate the experimental values of $\hat{q}$ from RHIC and LHC.

T (GeV)	$\hat{q}_{\rm SYM}$	$\phi_M=1$	$\phi_M=3$	$\phi_M=10$	Data
0.37	1.51	1.19	0.87	0.79	1.2 ± 0.3
0.47	3.10	2.54	2.20	2.15	1.9 ± 0.7

Table 1. Comparison between the jet quenching values obtained from $\mathcal{N}=4$ SYM, non-conformal model and experiments. Selected temperature are $T=0.37\,\text{GeV}$ (RHIC) and $T=0.47\,\text{GeV}$ (LHC).

experimental data. It is found that at $T=0.37\,\text{GeV}$ varying ϕ_M from 1 to 3 decreases $\hat{q}$ by $\sim 26\%$ while varying ϕ_M from 3 to 10 reduces $\hat{q}$ just about $\sim 9\%$. On the other hand, at $T=0.47\,\text{GeV}$ varying ϕ_M from 1 to 3, the decrease of $\hat{q}$ is about $\sim 13\%$ while varying ϕ_M from 3 to 10, the decrease of $\hat{q}$ is about $\sim 2\%$. Therefore, our results imply an increase of the jet-medium interaction at lower temperature where non-conformality effects are dominanat.

Holographic models such as [65, 73] indicate that increasing nonconformality leads to decreasing the value of jet quenching parameter which is consistence with our results from jet quenching parameter as well as the results of light quark stopping distance obtained from the previous section. In general, increasing the deviation from conformal invariance decreases the capability of medium to quench the jets of quarks. However, in the case of holographic QCD models with phase transition, this parameter exhibits a peak around the QCD phase transition region due to the fact that the system degrees of freedom change rapidly from hadronic gas to QGP [90, 91].

5 Summary

The quark-gluon plasma produced in heavy ion collisions is a strongly coupled, non-conformal plasma as indicated by lattice data [38] and hydrodynamics calculations [39–42]. The gauge/gravity duality provides us the opportunity to study the hot plasma in a strongly coupled regime. Suppression of high energy partons produced at heavy ion collision with

JHEP03(2019)045

high transverse momentum is one of the interesting properties of this strongly-coupled plasma that can be investigated using the AdS/CFT correspondence. Although, previous studies show that suppression of jets with sensible energies in $\mathcal{N} = 4$ SYM theory is much larger than its experimental expectations [59, 61].

In this paper, we investigated the suppression of jet in the strongly-coupled non-conformal plasma in the framework of AdS/CFT correspondence. We considered a holographic five-dimensional model consisting of Einstein gravity coupled to a scalar field with a non-trivial potential which corresponds to a dual four-dimensional non-conformal gauge theory which exhibits a renormalization group flow between two different fixed points (located at UV and IR) at zero temperature [48]. The parameter ϕ_M indicates the deviation from conformality as shown in figure 1.

We considered a point-like initial condition string created close to the boundary with endpoints that are free to fly apart. The initial conditions of the string are chosen such that the string extends in a direction parallel to the boundary as it falls toward the black hole horizon (falling string). The equations of motion for the string moving in the non-conformal background have been solved numerically and plotted in figure 2 for a typical string moving in the background with $\phi_M = 3$. Since the dynamics of the string depends on the string initial conditions (see figure 3, figure 5 and figure 6 for clarifications), we studied the maximum stopping distance which is insensitive to these IC in the string side. Although, this quantity is not good enough to compute the observables like nuclear modification factor, it is still a good quantity to estimate the stopping power of the plasma.

Our results show that the thermalization distance in the non-conformal backgrounds compare to the $\mathcal{N} = 4$ SYM theory depends on the fact that theories have the same temperature, figure 5 or the same entropy, figure 6. Actually, the figure 4 demonstrates that increasing non-conformality while keeping the entropy constant leads to a hotter plasma and consequently a larger jet suppression. We fitted the maximum stopping distance to the well-known relation presented in eq. (3.14) and used the n_{eff} as the stopping power of the plasma. Our numerical results, presented in figure 7 indicated that the thermalization distance increases by increasing the non-conformality of the plasma.

In the last section, we calculated the jet quenching parameter for the non-conformal geometry of section 2. For different values of ϕ_M, our results are in a good agreement with experimental data. Deviations from conformality are magnificent at lower temperatures and suppress at higher temperatures where non-conformal results approach to the corresponding value of the conformal background. As non-conformality increases, the value of jet quenching parameter decreases and this behavior is in consistency with both experiments and the results of light quark stopping distance obtained in section 3.2.

Acknowledgments

The authors wish to thank Hesam Soltanpanahi for the useful discussions. R. Morad also wishes to thank Prof. M. Maaza and iThemba LABS for the generous support and hospitality.

JHEP03(2019)045

References

[1] STAR collaboration, *Experimental and theoretical challenges in the search for the quark gluon plasma: The STAR Collaboration's critical assessment of the evidence from RHIC collisions*, *Nucl. Phys.* **A 757** (2005) 102 [nucl-ex/0501009] [INSPIRE].

[2] PHENIX collaboration, *Formation of dense partonic matter in relativistic nucleus-nucleus collisions at RHIC: Experimental evaluation by the PHENIX collaboration*, *Nucl. Phys.* **A 757** (2005) 184 [nucl-ex/0410003] [INSPIRE].

[3] BRAHMS collaboration, *Quark gluon plasma and color glass condensate at RHIC? The Perspective from the BRAHMS experiment*, *Nucl. Phys.* **A 757** (2005) 1 [nucl-ex/0410020] [INSPIRE].

[4] B.B. Back et al., *The PHOBOS perspective on discoveries at RHIC*, *Nucl. Phys.* **A 757** (2005) 28 [nucl-ex/0410022] [INSPIRE].

[5] G. Policastro, D.T. Son and A.O. Starinets, *The Shear viscosity of strongly coupled $N = 4$ supersymmetric Yang-Mills plasma*, *Phys. Rev. Lett.* **87** (2001) 081601 [hep-th/0104066] [INSPIRE].

[6] P. Kovtun, D.T. Son and A.O. Starinets, *Viscosity in strongly interacting quantum field theories from black hole physics*, *Phys. Rev. Lett.* **94** (2005) 111601 [hep-th/0405231] [INSPIRE].

[7] R. Baier, Y.L. Dokshitzer, A.H. Mueller, S. Peigne and D. Schiff, *Radiative energy loss of high-energy quarks and gluons in a finite volume quark-gluon plasma*, *Nucl. Phys.* **B 483** (1997) 291 [hep-ph/9607355] [INSPIRE].

[8] K.J. Eskola, H. Honkanen, C.A. Salgado and U.A. Wiedemann, *The Fragility of high-p_T hadron spectra as a hard probe*, *Nucl. Phys.* **A 747** (2005) 511 [hep-ph/0406319] [INSPIRE].

[9] J.M. Maldacena, *The Large N limit of superconformal field theories and supergravity*, *Int. J. Theor. Phys.* **38** (1999) 1113 [hep-th/9711200] [INSPIRE].

[10] E. Witten, *Anti-de Sitter space and holography*, *Adv. Theor. Math. Phys.* **2** (1998) 253 [hep-th/9802150] [INSPIRE].

[11] S.S. Gubser, I.R. Klebanov and A.M. Polyakov, *Gauge theory correlators from noncritical string theory*, *Phys. Lett.* **B 428** (1998) 105 [hep-th/9802109] [INSPIRE].

[12] O. Aharony, S.S. Gubser, J.M. Maldacena, H. Ooguri and Y. Oz, *Large N field theories, string theory and gravity*, *Phys. Rept.* **323** (2000) 183 [hep-th/9905111] [INSPIRE].

[13] J. Casalderrey-Solana, H. Liu, D. Mateos, K. Rajagopal and U.A. Wiedemann, *Gauge/String Duality, Hot QCD and Heavy Ion Collisions*, arXiv:1101.0618 [INSPIRE].

[14] E. Shuryak, *Physics of Strongly coupled quark-gluon Plasma*, *Prog. Part. Nucl. Phys.* **62** (2009) 48 [arXiv:0807.3033] [INSPIRE].

[15] E.V. Shuryak, *What RHIC experiments and theory tell us about properties of quark-gluon plasma?*, *Nucl. Phys.* **A 750** (2005) 64 [hep-ph/0405066] [INSPIRE].

JHEP03(2019)045

[16] P. Kovtun, D.T. Son and A.O. Starinets, *Holography and hydrodynamics: Diffusion on stretched horizons*, *JHEP* **10** (2003) 064 [hep-th/0309213] [INSPIRE].

[17] A. Buchel and J.T. Liu, *Universality of the shear viscosity in supergravity*, *Phys. Rev. Lett.* **93** (2004) 090602 [hep-th/0311175] [INSPIRE].

[18] D. Teaney, *The Effects of viscosity on spectra, elliptic flow and HBT radii*, *Phys. Rev.* **C 68** (2003) 034913 [nucl-th/0301099] [INSPIRE].

[19] STAR collaboration, *Elliptic flow in $Au + Au$ collisions at $\sqrt{s_{NN}} = 130$ GeV*, *Phys. Rev. Lett.* **86** (2001) 402 [nucl-ex/0009011] [INSPIRE].

[20] PHENIX collaboration, *Elliptic flow of identified hadrons in $Au + Au$ collisions at $\sqrt{s_{NN}} = 200$-GeV*, *Phys. Rev. Lett.* **91** (2003) 182301 [nucl-ex/0305013] [INSPIRE].

[21] PHOBOS collaboration, *Centrality and pseudorapidity dependence of elliptic flow for charged hadrons in $Au + Au$ collisions at $\sqrt{s_{NN}} = 200$-GeV*, *Phys. Rev.* **C 72** (2005) 051901 [nucl-ex/0407012] [INSPIRE].

[22] ATLAS collaboration, *Measurement of the azimuthal anisotropy for charged particle production in $\sqrt{s_{NN}} = 2.76$ TeV lead-lead collisions with the ATLAS detector*, *Phys. Rev.* **C 86** (2012) 014907 [arXiv:1203.3087] [INSPIRE].

[23] CMS collaboration, *Measurement of the elliptic anisotropy of charged particles produced in PbPb collisions at $\sqrt{s}_{NN} = 2.76$ TeV*, *Phys. Rev.* **C 87** (2013) 014902 [arXiv:1204.1409] [INSPIRE].

[24] ALICE collaboration, *Elliptic flow of charged particles in Pb-Pb collisions at 2.76 TeV*, *Phys. Rev. Lett.* **105** (2010) 252302 [arXiv:1011.3914] [INSPIRE].

[25] ALICE collaboration, *Anisotropic flow of charged particles in Pb-Pb collisions at $\sqrt{s_{\rm NN}} = 5.02$ TeV*, *Phys. Rev. Lett.* **116** (2016) 132302 [arXiv:1602.01119] [INSPIRE].

[26] ATLAS collaboration, *Measurement of long-range pseudorapidity correlations and azimuthal harmonics in $\sqrt{s_{NN}} = 5.02$ TeV proton-lead collisions with the ATLAS detector*, *Phys. Rev.* **C 90** (2014) 044906 [arXiv:1409.1792] [INSPIRE].

[27] CMS collaboration, *Evidence for Collective Multiparticle Correlations in p-Pb Collisions*, *Phys. Rev. Lett.* **115** (2015) 012301 [arXiv:1502.05382] [INSPIRE].

[28] ALICE collaboration, *Multiparticle azimuthal correlations in p-Pb and Pb-Pb collisions at the CERN Large Hadron Collider*, *Phys. Rev.* **C 90** (2014) 054901 [arXiv:1406.2474] [INSPIRE].

[29] ATLAS collaboration, *Observation of Long-Range Elliptic Azimuthal Anisotropies in $\sqrt{s} = 13$ and 2.76 TeV pp Collisions with the ATLAS Detector*, *Phys. Rev. Lett.* **116** (2016) 172301 [arXiv:1509.04776] [INSPIRE].

[30] M.P. Heller, R.A. Janik and P. Witaszczyk, *The characteristics of thermalization of boost-invariant plasma from holography*, *Phys. Rev. Lett.* **108** (2012) 201602 [arXiv:1103.3452] [INSPIRE].

[31] P.M. Chesler and L.G. Yaffe, *Boost invariant flow, black hole formation and far-from-equilibrium dynamics in $N = 4$ supersymmetric Yang-Mills theory*, *Phys. Rev.* **D 82** (2010) 026006 [arXiv:0906.4426] [INSPIRE].

[32] P.M. Chesler and L.G. Yaffe, *Holography and off-center collisions of localized shock waves*, *JHEP* **10** (2015) 070 [arXiv:1501.04644] [INSPIRE].

JHEP03(2019)045

[33] P.M. Chesler and L.G. Yaffe, *Numerical solution of gravitational dynamics in asymptotically anti-de Sitter spacetimes*, *JHEP* **07** (2014) 086 [arXiv:1309.1439] [INSPIRE].

[34] J. Casalderrey-Solana, M.P. Heller, D. Mateos and W. van der Schee, *Longitudinal Coherence in a Holographic Model of Asymmetric Collisions*, *Phys. Rev. Lett.* **112** (2014) 221602 [arXiv:1312.2956] [INSPIRE].

[35] J. Casalderrey-Solana, M.P. Heller, D. Mateos and W. van der Schee, *From full stopping to transparency in a holographic model of heavy ion collisions*, *Phys. Rev. Lett.* **111** (2013) 181601 [arXiv:1305.4919] [INSPIRE].

[36] P.M. Chesler, *How big are the smallest drops of quark-gluon plasma?*, *JHEP* **03** (2016) 146 [arXiv:1601.01583] [INSPIRE].

[37] P.M. Chesler, *Colliding shock waves and hydrodynamics in small systems*, *Phys. Rev. Lett.* **115** (2015) 241602 [arXiv:1506.02209] [INSPIRE].

[38] S. Ryu et al., *Importance of the Bulk Viscosity of QCD in Ultrarelativistic Heavy-Ion Collisions*, *Phys. Rev. Lett.* **115** (2015) 132301 [arXiv:1502.01675] [INSPIRE].

[39] P. Bozek, *Collective flow in p-Pb and d-Pd collisions at TeV energies*, *Phys. Rev.* **C 85** (2012) 014911 [arXiv:1112.0915] [INSPIRE].

[40] B. Schenke and R. Venugopalan, *Eccentric protons? Sensitivity of flow to system size and shape in p+p, p+Pb and Pb+Pb collisions*, *Phys. Rev. Lett.* **113** (2014) 102301 [arXiv:1405.3605] [INSPIRE].

[41] M. Habich, G.A. Miller, P. Romatschke and W. Xiang, *Testing hydrodynamic descriptions of p+p collisions at* $\sqrt{s} = 7$ *TeV*, *Eur. Phys. J.* **C 76** (2016) 408 [arXiv:1512.05354] [INSPIRE].

[42] S. Jeon and U. Heinz, *Introduction to Hydrodynamics*, *Int. J. Mod. Phys.* **E 24** (2015) 1530010 [arXiv:1503.03931] [INSPIRE].

[43] J. Polchinski and M.J. Strassler, *The String dual of a confining four-dimensional gauge theory*, hep-th/0003136 [INSPIRE].

[44] A. Karch and E. Katz, *Adding flavor to AdS/CFT*, *JHEP* **06** (2002) 043 [hep-th/0205236] [INSPIRE].

[45] T. Sakai and S. Sugimoto, *Low energy hadron physics in holographic QCD*, *Prog. Theor. Phys.* **113** (2005) 843 [hep-th/0412141] [INSPIRE].

[46] U. Gürsoy and E. Kiritsis, *Exploring improved holographic theories for QCD: Part I*, *JHEP* **02** (2008) 032 [arXiv:0707.1324] [INSPIRE].

[47] B. Galow, E. Megias, J. Nian and H.J. Pirner, *Phenomenology of AdS/QCD and its gravity dual*, *Nucl. Phys.* **B 834** (2010) 330 [arXiv:0911.0627] [INSPIRE].

[48] M. Attems et al., *Thermodynamics, transport and relaxation in non-conformal theories*, *JHEP* **10** (2016) 155 [arXiv:1603.01254] [INSPIRE].

[49] S.S. Gubser and A. Nellore, *Mimicking the QCD equation of state with a dual black hole*, *Phys. Rev.* **D 78** (2008) 086007 [arXiv:0804.0434] [INSPIRE].

[50] ALICE collaboration, *Elliptic flow of strange and multi-strange particles in Pb-Pb collisions at* $\sqrt{s_{NN}} = 2.76$*-TeV measured with ALICE*, *Acta Phys. Polon. Supp.* **6** (2013) 479 [INSPIRE].

JHEP03(2019)045

[51] ATLAS collaboration, *Observation of a Centrality-Dependent Dijet Asymmetry in Lead-Lead Collisions at $\sqrt{s_{NN}} = 2.77$ TeV with the ATLAS Detector at the LHC*, *Phys. Rev. Lett.* **105** (2010) 252303 [arXiv:1011.6182] [INSPIRE].

[52] CMS collaboration, *Observation and studies of jet quenching in PbPb collisions at nucleon-nucleon center-of-mass energy = 2.76 TeV*, *Phys. Rev.* **C 84** (2011) 024906 [arXiv:1102.1957] [INSPIRE].

[53] C.P. Herzog, A. Karch, P. Kovtun, C. Kozcaz and L.G. Yaffe, *Energy loss of a heavy quark moving through $N = 4$ supersymmetric Yang-Mills plasma*, *JHEP* **07** (2006) 013 [hep-th/0605158] [INSPIRE].

[54] S.S. Gubser, *Drag force in AdS/CFT*, *Phys. Rev.* **D 74** (2006) 126005 [hep-th/0605182] [INSPIRE].

[55] W.A. Horowitz and Y.V. Kovchegov, *Shock Treatment: Heavy Quark Drag in a Novel AdS Geometry*, *Phys. Lett.* **B 680** (2009) 56 [arXiv:0904.2536] [INSPIRE].

[56] K. Bitaghsir Fadafan, H. Liu, K. Rajagopal and U.A. Wiedemann, *Stirring Strongly Coupled Plasma*, *Eur. Phys. J.* **C 61** (2009) 553 [arXiv:0809.2869] [INSPIRE].

[57] W.A. Horowitz, *Fluctuating heavy quark energy loss in a strongly coupled quark-gluon plasma*, *Phys. Rev.* **D 91** (2015) 085019 [arXiv:1501.04693] [INSPIRE].

[58] P.M. Chesler, K. Jensen, A. Karch and L.G. Yaffe, *Light quark energy loss in strongly-coupled $N = 4$ supersymmetric Yang-Mills plasma*, *Phys. Rev.* **D 79** (2009) 125015 [arXiv:0810.1985] [INSPIRE].

[59] R. Morad and W.A. Horowitz, *Strong-coupling Jet Energy Loss from AdS/CFT*, *JHEP* **11** (2014) 017 [arXiv:1409.7545] [INSPIRE].

[60] A. Ficnar, J. Noronha and M. Gyulassy, *Jet Quenching in Non-Conformal Holography*, *J. Phys.* **G 38** (2011) 124176 [arXiv:1106.6303] [INSPIRE].

[61] K. Bitaghsir Fadafan and R. Morad, *Jets in a strongly coupled anisotropic plasma*, *Eur. Phys. J.* **C 78** (2018) 16 [arXiv:1710.06417] [INSPIRE].

[62] F. D'Eramo, H. Liu and K. Rajagopal, *Transverse Momentum Broadening and the Jet Quenching Parameter, Redux*, *Phys. Rev.* **D 84** (2011) 065015 [arXiv:1006.1367] [INSPIRE].

[63] H. Liu, K. Rajagopal and U.A. Wiedemann, *Wilson loops in heavy ion collisions and their calculation in AdS/CFT*, *JHEP* **03** (2007) 066 [hep-ph/0612168] [INSPIRE].

[64] E. Caceres and A. Guijosa, *On Drag Forces and Jet Quenching in Strongly Coupled Plasmas*, *JHEP* **12** (2006) 068 [hep-th/0606134] [INSPIRE].

[65] A. Buchel, *On jet quenching parameters in strongly coupled non-conformal gauge theories*, *Phys. Rev.* **D 74** (2006) 046006 [hep-th/0605178] [INSPIRE].

[66] J.F. Vazquez-Poritz, *Enhancing the jet quenching parameter from marginal deformations*, hep-th/0605296 [INSPIRE].

[67] E. Nakano, S. Teraguchi and W.-Y. Wen, *Drag force, jet quenching and AdS/QCD*, *Phys. Rev.* **D 75** (2007) 085016 [hep-ph/0608274] [INSPIRE].

[68] S.D. Avramis and K. Sfetsos, *Supergravity and the jet quenching parameter in the presence of R-charge densities*, *JHEP* **01** (2007) 065 [hep-th/0606190] [INSPIRE].

[69] Y.-h. Gao, W.-s. Xu and D.-f. Zeng, *Jet quenching parameters of Sakai-Sugimoto Model*, hep-th/0611217 [INSPIRE].

JHEP03(2019)045

[70] N. Armesto, J.D. Edelstein and J. Mas, *Jet quenching at finite 't Hooft coupling and chemical potential from AdS/CFT*, *JHEP* **09** (2006) 039 [hep-ph/0606245] [INSPIRE].

[71] F.-L. Lin and T. Matsuo, *Jet Quenching Parameter in Medium with Chemical Potential from AdS/CFT*, *Phys. Lett.* **B 641** (2006) 45 [hep-th/0606136] [INSPIRE].

[72] J. Sadeghi and S. Heshmatian, *Jet Quenching Parameter with Hyperscaling Violation*, *Eur. Phys. J.* **C 74** (2014) 3032 [arXiv:1308.5991] [INSPIRE].

[73] U. Gursoy, E. Kiritsis, L. Mazzanti, G. Michalogiorgakis and F. Nitti, *Improved Holographic QCD*, *Lect. Notes Phys.* **828** (2011) 79 [arXiv:1006.5461].

[74] R.-G. Cai, S. Chakrabortty, S. He and L. Li, *Some aspects of QGP phase in a hQCD model*, *JHEP* **02** (2013) 068 [arXiv:1209.4512] [INSPIRE].

[75] L. Wang and S.-Y. Wu, *Holographic study of the jet quenching parameter in anisotropic systems*, *Eur. Phys. J.* **C 76** (2016) 587 [arXiv:1609.03665] [INSPIRE].

[76] O. DeWolfe and C. Rosen, *Robustness of Sound Speed and Jet Quenching for Gauge/Gravity Models of Hot QCD*, *JHEP* **07** (2009) 022 [arXiv:0903.1458] [INSPIRE].

[77] K. Bitaghsir Fadafan, *Charge effect and finite 't Hooft coupling correction on drag force and Jet Quenching Parameter*, *Eur. Phys. J.* **C 68** (2010) 505 [arXiv:0809.1336] [INSPIRE].

[78] W.A. Horowitz, *Time Dependent $\hat{q}$ from AdS/CFT*, *Nucl. Part. Phys. Proc.* **289-290** (2017) 129 [INSPIRE].

[79] M. Bianchi, D.Z. Freedman and K. Skenderis, *Holographic renormalization*, *Nucl. Phys.* **B 631** (2002) 159 [hep-th/0112119] [INSPIRE].

[80] J. Mas and J. Tarrio, *Hydrodynamics from the Dp-brane*, *JHEP* **05** (2007) 036 [hep-th/0703093] [INSPIRE].

[81] P.M. Chesler, K. Jensen and A. Karch, *Jets in strongly-coupled $N = 4$ super Yang-Mills theory*, *Phys. Rev.* **D 79** (2009) 025021 [arXiv:0804.3110] [INSPIRE].

[82] B.G. Zakharov, *Radiative energy loss of high-energy quarks in finite size nuclear matter and quark-gluon plasma*, *JETP Lett.* **65** (1997) 615 [hep-ph/9704255] [INSPIRE].

[83] J.M. Maldacena, *Wilson loops in large N field theories*, *Phys. Rev. Lett.* **80** (1998) 4859 [hep-th/9803002] [INSPIRE].

[84] S.-J. Rey and J.-T. Yee, *Macroscopic strings as heavy quarks in large N gauge theory and anti-de Sitter supergravity*, *Eur. Phys. J.* **C 22** (2001) 379 [hep-th/9803001] [INSPIRE].

[85] S.-J. Rey, S. Theisen and J.-T. Yee, *Wilson-Polyakov loop at finite temperature in large N gauge theory and anti-de Sitter supergravity*, *Nucl. Phys.* **B 527** (1998) 171 [hep-th/9803135] [INSPIRE].

[86] A. Brandhuber, N. Itzhaki, J. Sonnenschein and S. Yankielowicz, *Wilson loops in the large N limit at finite temperature*, *Phys. Lett.* **B 434** (1998) 36 [hep-th/9803137] [INSPIRE].

[87] J. Sonnenschein, *What does the string/gauge correspondence teach us about Wilson loops?*, in *Supersymmetry in the theories of fields, strings and branes. Proceedings of Advanced School*, Santiago de Compostela Spain (1999), pg. 219 [hep-th/0003032] [INSPIRE].

[88] H. Liu, K. Rajagopal and U.A. Wiedemann, *Calculating the jet quenching parameter from AdS/CFT*, *Phys. Rev. Lett.* **97** (2006) 182301 [hep-ph/0605178] [INSPIRE].

JHEP03(2019)045

[89] JET collaboration, *Extracting the jet transport coefficient from jet quenching in high-energy heavy-ion collisions*, *Phys. Rev.* **C 90** (2014) 014909 [arXiv:1312.5003] [INSPIRE].

[90] R. Rougemont, A. Ficnar, S. Finazzo and J. Noronha, *Energy loss, equilibration and thermodynamics of a baryon rich strongly coupled quark-gluon plasma*, *JHEP* **04** (2016) 102 [arXiv:1507.06556] [INSPIRE].

[91] D. Li, J. Liao and M. Huang, *Enhancement of jet quenching around phase transition: result from the dynamical holographic model*, *Phys. Rev.* **D 89** (2014) 126006 [arXiv:1401.2035] [INSPIRE].

JHEP03(2019)045